MOLECULAR AND CELLULAR BIOLOGY
2023, VOL. 43, NO. 4, 143–156
https://doi.org/10.1080/10985549.2023.2196204

Taylor & Francis
Taylor & Francis Group

RESEARCH ARTICLE

DNA Damage-Induced, S-Phase Specific Phosphorylation of Orc6 is Critical for the Maintenance of Genome Stability

Yo-Chuen Lin,* Dazhen Liu,* Arindam Chakraborty,* Virgilia Macias, Eileen Brister, Jay Sonalkar, Linyuan Shen, Jaba Mitra, Taekjip Ha, Andre Kajdacsy-Balla, Kannanganattu V. Prasanth, Supriya G. Prasanth

[a]Department of Cell and Developmental Biology, University of Illinois at Urbana-Champaign, Urbana, Illinois, USA
[b]Research Tissue Imaging Core, Department of Pathology, University of Illinois, Chicago, Illinois, USA
[c]Biophysics and Biophysical Chemistry, Johns Hopkins University, Baltimore, Maryland, USA
[d]Howard Hughes Medical Institute, Johns Hopkins University, Baltimore, Maryland, USA
[e]Cancer Center at Illinois, UIUC, Urbana, Illinois, USA

ABSTRACT The smallest subunit of the human Origin Recognition Complex, hOrc6, is required for DNA replication progression and plays an important role in mismatch repair (MMR) during S-phase. However, the molecular details of how hOrc6 regulates DNA replication and DNA damage response remain to be elucidated. Orc6 levels are elevated upon specific types of genotoxic stress, and it is phosphorylated at Thr229, predominantly during S-phase, in response to oxidative stress. Many repair pathways, including MMR, mediate oxidative DNA damage repair. Defects in MMR are linked to Lynch syndrome, predisposing patients to many cancers, including colorectal cancer. Orc6 levels are known to be elevated in colorectal cancers. Interestingly, tumor cells show reduced hOrc6-Thr229 phosphorylation compared to adjacent normal mucosa. Further, elevated expression of wild-type and the phospho-dead forms of Orc6 results in increased tumorigenicity, implying that in the absence of this "checkpoint" signal, cells proliferate unabated. Based on these results, we propose that DNA-damage-induced hOrc6-pThr229 phosphorylation during S-phase facilitates ATR signaling in the S-phase, halts fork progression, and enables assembly of repair factors to mediate efficient repair to prevent tumorigenesis. Our study provides novel insights into how hOrc6 regulates genome stability.

KEYWORDS DNA damage, Orc6, phosphorylation, replication

INTRODUCTION

The assembly of pre-replication complex (pre-RC), the first step for setting up a DNA replication program, is a stepwise event that starts from the binding of the origin recognition complex (ORC) to the origins of DNA replication during the G1 phase.[1,2] Orc6, the smallest subunit of ORC, is an essential factor regulating cell cycle progression. As a part of ORC, studies from yeast to *Drosophila* point out that Orc6 is critical for origin recognition and licensing in the G1 phase.[3–5] Surprisingly, our previous finding revealed that human Orc6 (hOrc6) is dispensable in the licensing process.[6] Rather, we identified an unexpected role of hOrc6 in supporting S phase progression and DNA damage response (DDR). However, the mechanism of how Orc6 regulates S phase progression and DDR is unclear. Moreover, metazoan Orc6 is reported to function in cytokinesis, and hOrc6 facilitates MMR activity.[6–9] All these studies among different species highlight the multifunctional and evolutionarily divergent role of Orc6.

DNA replication is coordinated with the DDR network to maintain genome stability.[10] ATM (ataxia-telangiectasia mutated) and ATR (ATM and Rad3-related) are the key kinases that regulate DDR.[11] While ATM activation requires a double-strand

Address correspondence to Supriya G. Prasanth, supriyap@illinois.edu
*Authors contributed equally.
The authors declare no conflict of interest.

Received 7 October 2022
Revised 16 February 2023
Accepted 17 February 2023

DNA break bound by the MRN complex,[12] ATR is typically activated in association with its partner ATRIP when it senses single-stranded DNA coated by RPA.[11,13] ATM/ATR and their downstream effector kinases, Chk2 and Chk1, activate checkpoints to stop cell cycle progression and allow damaged DNA to be repaired. Even though different types of damage activate these checkpoints, there is considerable crosstalk between these pathways.[14,15] ATR and Chk1 restrain replication origin firing in normal cells as well as after DNA damage. Further, dormant origins are reported to fire in cells lacking Chk1, suggesting that ATR-Chk1 control the firing of dormant origins.[16,17] Subunits of ORC, ORCA/LRWD1, Cdc6, and multiple MCM subunits are potential substrates of ATM and ATR.[18] In addition, multiple pre-RC proteins interact with the components of the ATR pathway, and yet the functional relevance of such interaction remains to be understood.

We report here that the levels of hOrc6 increase upon DNA damage, and hOrc6 undergoes specific phosphorylation upon oxidative DNA damage. Using phospho-mimetic and phospho-dead mutants, we characterized the functional relevance of hOrc6 phosphorylation in S phase progression. Human Orc6 preferentially binds to replication fork-like DNA structures, and the depletion of hOrc6 causes defects in S-phase, as evidenced by shorter IdU track lengths. Expression of WT and phospho-dead mutant of Orc6 efficiently rescues this defect, but not the phospho-mimetic mutant of Orc6. Moreover, we show that this phosphorylation is a downstream target of ATR and is involved in ATR signaling activation. Orc6 upregulation is correlated with poor prognosis in many different tumors. We find that hOrc6 promotes migratory and invasive properties of tumor cells. The phosphorylated hOrc6 shows reduced levels in tumors compared to normal mucosa supporting our model that hOrc6 phosphorylation is important for fork halting to enable DNA repair. Our study provides novel insights into how hOrc6 regulates genome stability.

RESULTS

Orc6 is upregulated and phosphorylated in response to oxidative stress during S-Phase. In yeast, Orc6 is phosphorylated in a cell cycle-dependent manner, with increased Orc6 phosphorylation as the cells exit G1. The hyperphosphorylation of yOrc6 following START is one of the known mechanisms by which cells prevent re-replication.[19] We have observed that a population of hOrc6 is phosphorylated upon DNA damage. We successfully mapped the DNA damage-mediated phosphorylation site of hOrc6 at T229 by performing PhosTag gel electrophoresis[20] (Fig. 1A). In addition, we have also observed another phosphorylation at the T195 moiety, reported previously.[21] U2OS cells were transfected with Flag-Orc6-WT, T195A, T229A or M2 (both T195 and T229 were mutated to Ala) and treated with okadaic acid to induce the accumulation of the phosphorylation. In cells transfected with Flag-Orc6-WT, four major bands were noticeable (unphosphorylated, * corresponding to Orc6 phosphorylated on both T195 and T229; *1 indicating T229 phosphorylation, *2 indicating T195 phosphorylation). Calf intestinal phosphatase (CIP) treatment confirmed the phosphorylation at these sites.

We further investigated hOrc6 T229 phosphorylation (pT229) by generating an antibody that specifically recognized only the pT229-modified version of hOrc6. Cells were treated with different DNA-damaging agents. The most robust phosphorylation at Orc6-T229 was found in cells treated with oxidative damage-inducing agents such as okadaic acid (a phosphatase inhibitor, also a potent inducer of cellular H_2O_2) and H_2O_2 (Fig. 1A to C). Phosphorylation of T229 was also observed when cells were treated with UV, NCS (neocarzinostatin, generating free radicals), and methyl methanesulfonate (MMS, to varying extents in different experiments), and during early stages of gamma irradiation in asynchronous cells (Fig. 1B and C). Interestingly, oxidative stress-responsive pT229 of hOrc6 was increased preferentially during the S-phase (Fig. 1D), suggesting a potential link of this phosphorylation to its S-phase function. Similarly, phosphorylation was observed when cells were treated with MMS during the S-phase (data not shown). We further tested the regulation of pT229 with different doses and

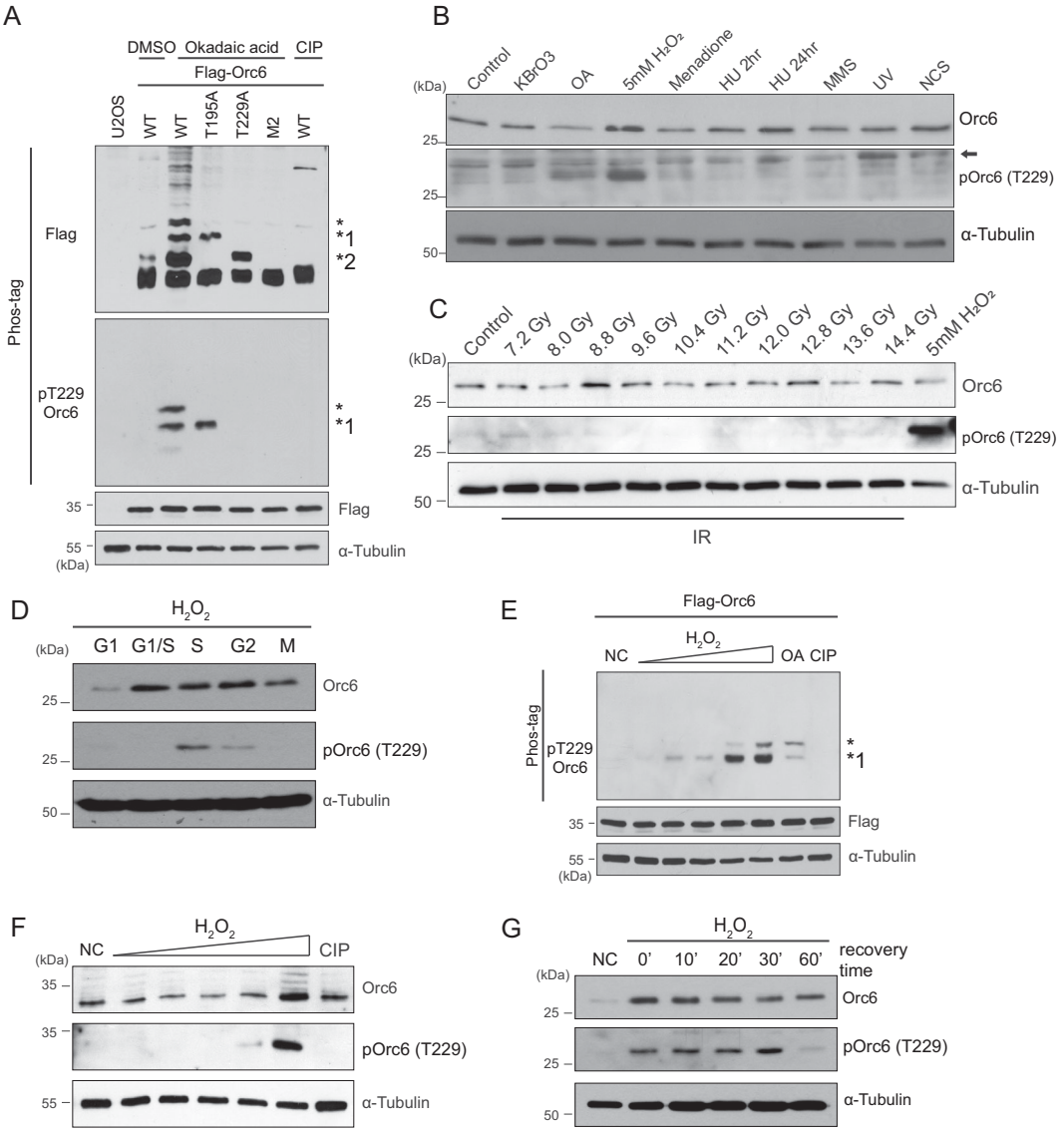

FIG 1 Orc6 is phosphorylated at threonine 229 (T229) upon oxidative damage during S-phase. (A) Phos-tag gel analysis of Orc6 phosphorylation. U2OS cells were transfected with Flag-Orc6-WT, T195A, T229A or M2 (both T195 and T229 were mutated to Ala) and treated with okadaic acid (OA) to induce accumulation of phosphorylation. Asterisk (*) indicates Orc6 phosphorylated on both T195 and T229; *1 indicates T229 phosphorylation. *2 indicates T195 phosphorylation. CIP, calf intestinal phosphatase. (B) Western blot for testing Orc6 T229 phosphorylation upon different genotoxic drug treatments. Arrowhead indicates nonspecific bands. (C) Western blot for testing Orc6 T229 phosphorylation upon different doses of gamma irradiation. (D) Western blot showing Orc6 T229 phosphorylation pattern during cell cycle. (E) Phos-tag gel analysis to determine the dose-dependent effects of T229 phosphorylation upon H_2O_2 treatment. U2OS cells were transfected with Flag-Orc6-WT and treated with different concentration of H_2O_2 (0.25, 0.5, 1, 2, 5 mM). NC: negative control. (F) Western blot for endogenous Orc6 T229 phosphorylation. (G) Western blot of T229 phosphorylation regulation after removal of 5 mM H_2O_2. Cells were collected at indicated time point after release from 20 min H_2O_2 treatment. NC: negative control.

time courses of H_2O_2 treatment. We observed that the phosphorylation at T229 depends on the dose of the damaging agent (Fig. 1E and F). Both the total and the pT229-modified levels of Orc6 were elevated upon oxidative stress (Fig. 1B, E to G). Treatment of cells with phosphatase (CIP) showed a loss of signal, confirming the specificity of the phospho-antibody (Fig. 1A, E and F). Strikingly, Orc6-pT229 was induced within 20 min of H_2O_2 treatment and persisted for ~30 min post-recovery from H_2O_2 release, following which the levels of Orc6-pT229 declined (Fig. 1G). Meanwhile, the cells recovered from H_2O_2 continued to show enhanced levels of total Orc6.

Unphosphorylated Orc6 facilitates fork progression. Orc6 is known to display robust DNA binding ability in metazoans.[22,23] In order to understand the types of DNA structure, which hOrc6 recognizes, we performed single molecule pull-down (SiMPull) assays.[24] We observed that hOrc6 bound more tightly to replication fork structures (Kd

6.34 ± 0.49 nM) compared to ssDNA (19.24 ± 5 nM) and dsDNA structures (15.82 ± 1.24 nM) (Fig. 2A and B). This is consistent with our previous observations that Orc6 localizes to the fork, interacts with the fork components, and plays an important role in S-phase progression.[6]

To address the role of Orc6-pT229 during S-phase, we investigated if Orc6-pT229 is present at the replication fork using in situ protein interactions at nascent replication forks (SIRF). SIRF utilizes the proximity ligation assay (PLA) procedure and detects the spatial proximity between the protein and biotinylated EdU at different locations. This procedure enables us to address if the target protein localizes at the nascent or mature chromatin. We used SIRF assay to study the association of Orc6-pT229 with biotinylated-EdU at nascent (EdU pulse for 10 min) and mature chromatin (4 h thymidine chase after EdU labeling) (Fig. 2C and D). Upon treatment of H_2O_2, Orc6-pT229 was present equally at the nascent and mature chromatin. These results support that Orc6-pT229, similar to unphosphorylated Orc6, can localize at the replication fork.

Since we have identified that hOrc6 binds to the replication fork and is involved in S-phase progression, the function of T229 phosphorylation upon oxidative stress during the S-phase and at the replication fork could imply that this phosphorylation may regulate/prevent fork progression under DNA damage conditions. It is worth noting that T229 is located adjacent to the "YxxWK" conserved motif within the C-terminus of hOrc6, the mutation of which is reported to impede the association of Orc6 with the core ORC and is linked to the Meier–Gorlin syndrome.[3] We, therefore, tested whether the hOrc6-pT229 affected Orc6's DNA binding activity and its interaction with other ORC subunits. We observed that both T229A and T229E mutants bound to DNA more efficiently than even the WT-Orc6, as observed by SiMPull assays (Fig. 2E and F). Also, the WT and both the mutants showed comparable levels of interaction with Orc2 using co-IP (Fig. 3A), suggesting that the T229 phosphorylation of hOrc6 does not alter its interaction with the DNA and ORC.

To study how the phospho-mutants impact cell cycle progression, we performed cell cycle experiments in control and hOrc6 knockout cells [hypomorph, (6)]. hOrc6 KO cells showed a reduced S-phase population, as expected (Fig. 3B, compare U2OS WT-NT [column 1, row 1] and Orc6 KO-NT [column 2, row 1]). The treatment of the control cells with H_2O_2, followed by their release post-treatment, showed efficient progression through the cell cycle (Fig. 3B, column 1). Expression of WT-Orc6 in the hOrc6-KO background rescued the cell cycle progression defects with cells progressing through S-phase. Similarly, the phospho-dead Orc6-T229A mutant could rescue the cell cycle defects phenotype upon Orc6 loss, albeit not as efficiently as the wild-type (Fig. 3B, columns 3–4). However, the expression of Orc6-T229E showed the least efficient progression through S-phase, suggesting that the phosphorylation prevented replication progression when the cells encounter DNA damage (Fig. 3B, column 5).

To assess the fork dynamics, we tested the function of hOrc6 in DNA replication by using a DNA combing assay.[25] Active replication forks were labeled by incorporating 5-chloro-2′-deoxyuridine (CldU) followed by 5-iodo-2′-deoxyUridine (IdU), and the DNA fiber length was measured to determine fork movement. We observed marginally shorter fibers in the absence of Orc6, suggesting that the fork velocity was slowed in the hOrc6-depleted cells (Fig. 3C). Further, expression of Orc6-WT resulted in increased speed and longer track lengths of IdU and rescued the slower fork progression observed in the Orc6-depleted cells (Fig. 3C). Similar rescue was observed in cells expressing the phospho-dead Orc6-T229A. However, the expression of Orc6-T229E showed track lengths like that observed in Orc6-depleted cells. Our results support the model that phosphorylation of Orc6 impacts fork progression.

Orc6 is a downstream target of ATR, and Orc6 T229 phosphorylation is important for ATR activation under oxidative stress. We had previously demonstrated that cells lacking hOrc6 failed to activate ATR upon oxidative stress.[6] The function of T229 could therefore be to facilitate DNA repair and DDR signal transduction directly. Indeed, using HA-Orc6 stable cell lines, we found that ATR activity (pChk1 and pRPA32) post-oxidative stress was partially rescued by both wild-type and T229E

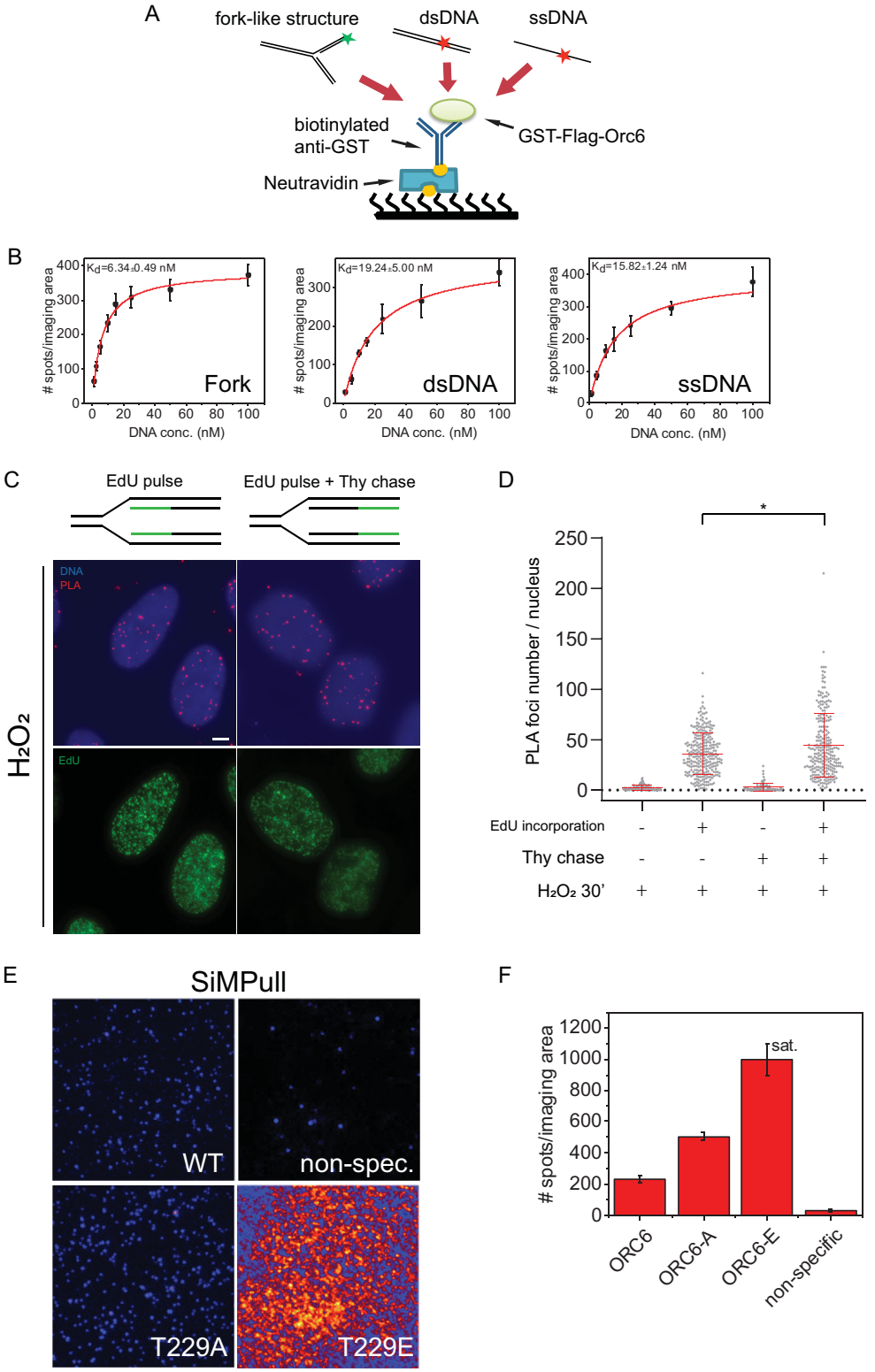

FIG 2 Orc6-pT229 binds to the replication fork. (A) Schematic illustration of SiMPull to test Orc6's DNA binding ability to different DNA substrates. (B) Binding curves showing Orc6 binding affinity to different DNA substrates. (C) Representative images of SIRF assay. Schematic of the experiment is provided. Scale bar, 5 μm. (D) Quantification of PLA foci number. EdU-positive and negative cells were processed and plotted separately. The quantification is based on two biological repeats of SIRF. Mean ± *SD*. $^{*}P < 0.05$, $^{****}P < 0.0001$ by Mann–Whitney U test. (E and F) SiMPull for investigating the effect of Orc6 T229 phosphorylation to its DNA fork structure binding ability. Representative images of different mutants of purified GST-Flag-Orc6 (E) and quantified results (F). Mean ± *SD*.

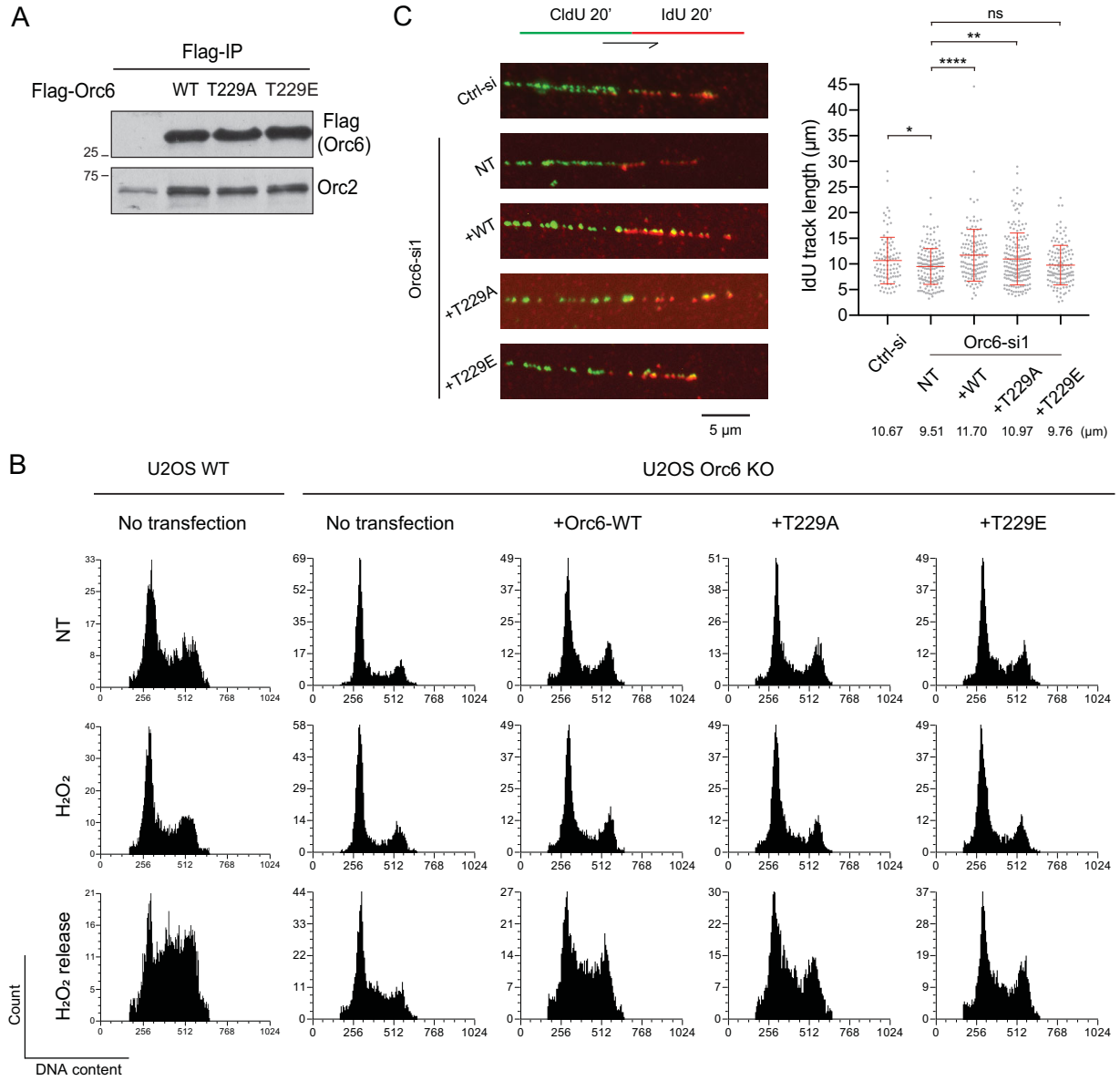

FIG 3 Impact of Orc6-pT229 on ORC binding, cell cycle progression and replication fork dynamics. (A) Immunoprecipitation of different mutants of Flag-Orc6 from U2OS cells. Samples were analyzed by Western blotting. (B) Cell cycle profile of U2OS cells (column 1) and Orc6-KO cells (columns 2–5) in cells expressing wild-type (column 3), phospho-dead (Orc6-T229A; column 4) or phospho-mimetic (Orc6-T229E; column 5) versions of Orc6. These cells were either untreated (NT), H_2O_2 treated or released from H_2O_2 treatment. (C) DNA fiber assay to monitor replication fork progression in cells expressing wild-type, phospho-dead or phospho-mimetic mutants of Orc6. Left: representative images. Schematic figure represents the CldU (green) and IdU (red) incorporation duration. Arrow indicates direction of replication. Scale bar, 5 μm. Right: quantification of IdU track length (μm) in unidirectional replication forks. Mean ± *SD*. In each sample $n = 99–188$ fibers were quantified. Numbers below represent mean values. $^{*}P < 0.05$, $^{**}P < 0.01$, $^{****}P < 0.0001$ by unpaired two-tailed Student's *t* test, and ns: nonsignificant.

mutant of Orc6-expressing cells but not the cells expressing T229A mutant (Fig. 4A). This result suggests that pT229 of Orc6 is important for activating the DDR network.

The T229 of hOrc6 is an ATM/ATR consensus (TQ/SQ) site, implying that DNA oxidative stress-induced phosphorylation of Orc6-T229 could be mediated by ATM/ATR axis. Interestingly, Orc6 T229 was identified as a potential downstream substrate of ATM/ATR in a proteomic screen.[18] To validate this, we performed ATR depletion and monitored Orc6 phosphorylation. We found that Orc6 phosphorylation at T229 was reduced in ATR-depleted cells, suggesting that pT229 is downstream of ATR (Fig. 4B). These data collectively indicate that Orc6 phosphorylation at T229 in response to DNA damage facilitates the ATR signaling pathway. The loss of T229 phosphorylation may

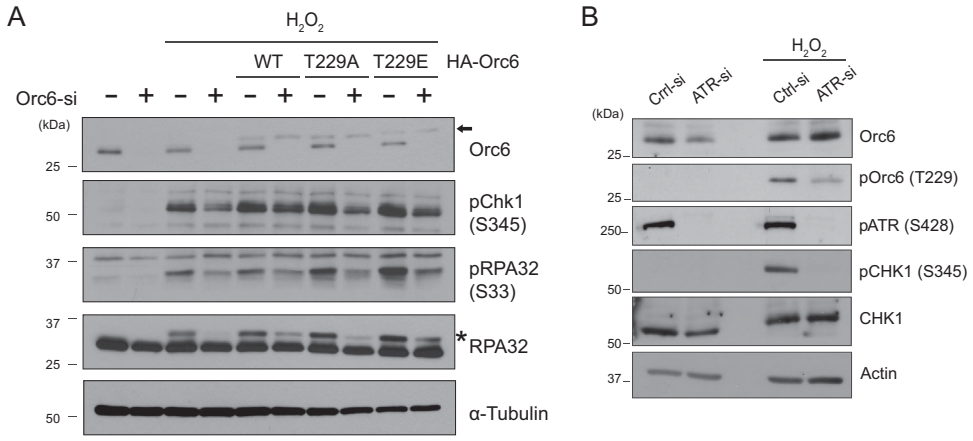

FIG 4 Orc6 phosphorylation at T229 upon oxidative damage is ATR-dependent. (A) ATR activation analyzed by Western blot of various U2OS cell lines (U2OS WT, HA-Orc6-WT, HA-Orc6-T229A, HA-Orc6-T229E) depleted of endogenous Orc6. Arrowhead indicates HA-Orc6. Asterisk (*) indicates hyperphosphorylated RPA32. Relative levels of hyperphosphorylated RPA32 (data normalized to the control si- 1; Orc6 si in U2OS WT- 0.17, in HA-Orc6 WT- 0.40, in HA-Orc6-T229A- 0.19, in HA-Orc6-T229E-0.51) and pChk1-S345 (data normalized to the control si- 1; Orc6 si in U2OS WT- 0.58, in HA-Orc6 WT- 1.03, in HA-Orc6-T229A- 0.63, in HA-Orc6-T229E- 0.79) in Orc6-si cells were quantified by ImageJ. (B) Western blot analysis of Orc6 phosphorylation at T229 upon ATR depletion.

cause the cells to fail to slow down the S-phase during oxidative stress, resulting in genome instability.

Depletion of Orc6 suppresses malignant phenotypes of cancer cells. Since Orc6 plays important roles in promoting S-phase progression and DDR, we investigated if it supports malignant behavior in cancer cells. Indeed, several earlier studies have reported that hOrc6 levels correlate with cancer progression and poor survival in several cancer types.[26–29] *ORC6* is also one of the genes used in multiple breast cancer gene expression profiling.[30] Further, it is upregulated in colorectal cancers,[31] and decreasing the levels of Orc6 in colorectal cancer cells causes them to become sensitive to chemotherapeutic drugs.[32] Defects in MMR pathway are often seen in colorectal tumors. Yet the molecular basis by which hOrc6 contributes to tumorigenesis remains unknown.

We found that *ORC6* is often amplified or mutated in different tumors (cBioPortal; Fig. 5A). Expression analysis of *ORC6L* across TCGA tumors (http://ualcan.path.uab.edu/) showed enhanced expression in various tumors (Fig. 5B). Finally, survival analysis revealed that higher expression of *ORC6* correlated with poor prognosis amongst various tumors (Fig. 5C).

To broaden the understanding of Orc6 in tumor progression, we performed a transwell migration assay of Orc6-depleted basal-like breast cancer cell line, M4 (MCF10CA1a.cl1) and U2OS cells, an osteosarcoma cell line. We observed that the depletion of Orc6 in cancer cells caused a significant reduction in cancer cell migration and invasion (Fig. 6A and B), suggesting that Orc6 is a critical player in promoting malignant cancer phenotypes. To gain mechanistic insights into the role of phosphorylation of Orc6 at T229 in tumorigenesis, we performed invasion and migration assays in cells expressing wild-type, the phospho-dead and the phospho-mimetic mutants of Orc6 (Fig. 6C and D). Our results demonstrated that the expression of Orc6-WT itself was sufficient to increase the cancer cells' invasion and migration properties. The expression of Orc6-T229A also drove migration and invasion to the same extent as WT-Orc6. The expression of Orc6-T229E, however, did not drive the migration to the same extent as the WT or 229A. This suggests that the unphosphorylated form of Orc6 promotes migration and invasion of tumor cells. In cells expressing the phospho-mimic mutant of Orc6, we find that the invasion and migration are not as pronounced as the expression of WT, suggesting that the phosphorylation of Orc6 could be a mechanism to prevent tumorigenic properties.

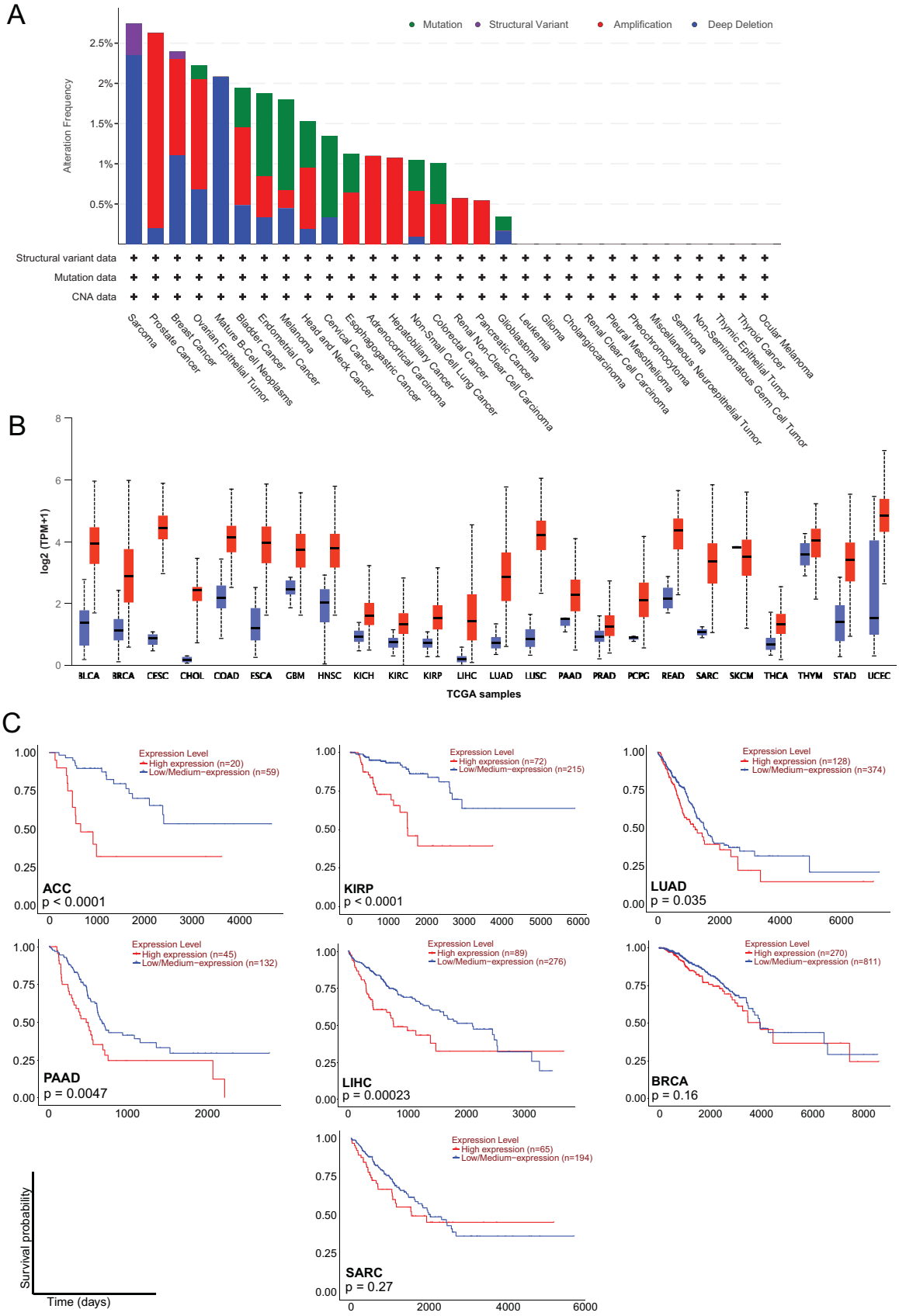

FIG 5 The significance of Orc6 in tumorigenesis. (A) Mutations, amplifications, and deletion of *ORC6L* in different tumors (cBioPortal). (B) Expression analysis of *ORC6L* across TCGA tumors (http://ualcan.path.uab.edu/). (C) Survival analysis in patients with higher *ORC6* expression levels (http://ualcan.path.uab.edu).

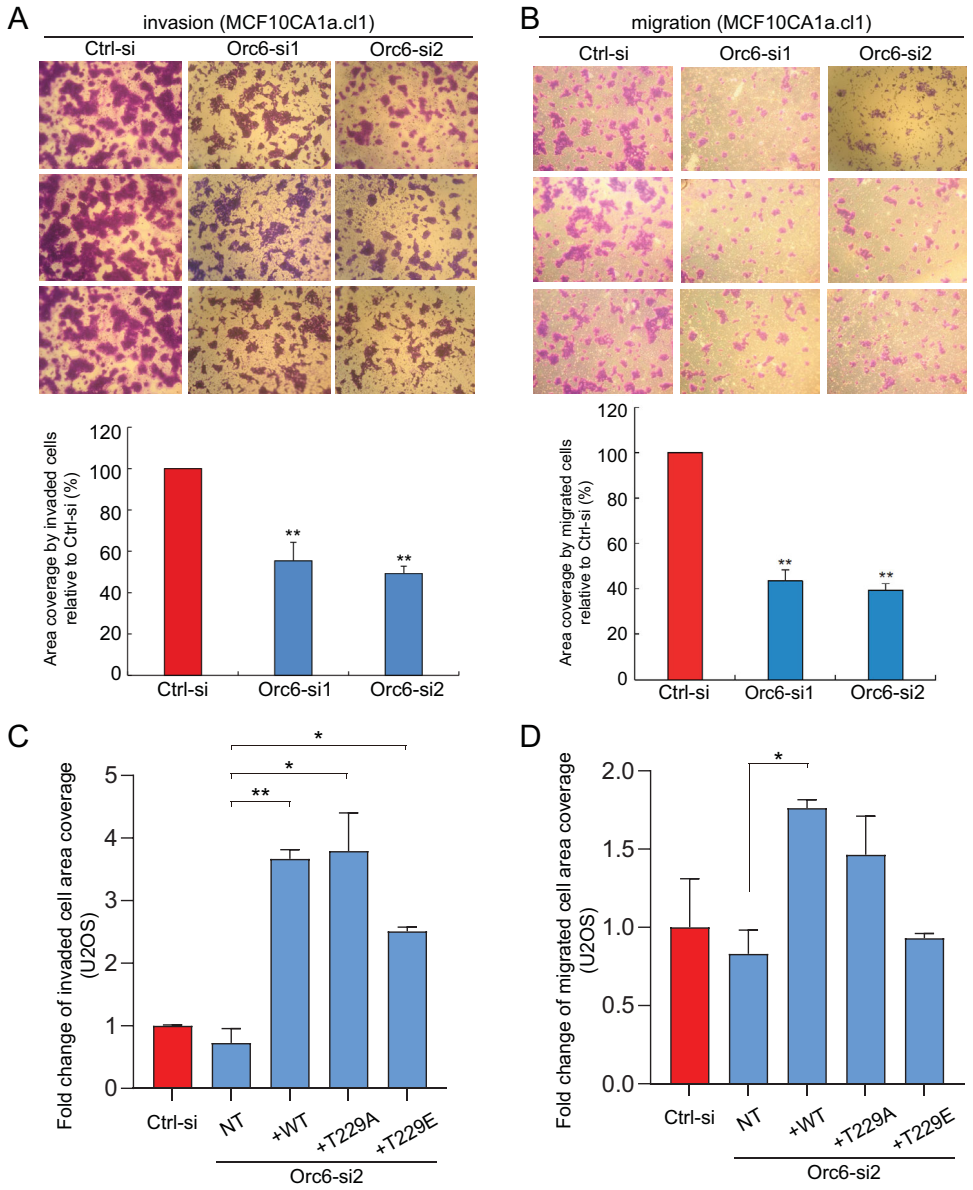

FIG 6 The role of Orc6-pT229 in tumorigenesis. (A) Matrigel invasion assay of Orc6-depleted M4 cells. (B) Transwell migration assay of Orc6-depleted M4 cells. (C and D) Invasion (C) and migration (D) assays of Orc6-depleted U2OS cells, in which endogenous Orc6 was substituted by HA-Orc6-WT/T229A/T229E. Quantification is based on area coverage by migrated or invaded cells stained by crystal violet. Mean ± SEM. $n = 2$ replicates. $^{*}P < 0.05$, $^{**}P < 0.01$ by unpaired two-tailed Student's t test. Unlisted p-values: (C) $P = 0.3590$ between Ctrl-si and Orc6-si2-NT; (D) $P = 0.6746$ between Ctrl-si and Orc6-si2-NT, $P = 0.1592$ between Orc6-si2-NT and Orc6-si2 + T229A, $P = 0.5835$ between Orc6-si2-NT and Orc6-si2 + T229E.

Finally, to understand the abundance of Orc6 pT229 in tumor cells, we performed immunohistochemistry analyses of Orc6 (Fig. 7A) and Orc6 pT229 (Fig. 7B) in colon cancer cells and evaluated their distribution. Orc6 showed a 7.7-fold higher signal intensity at the tumor sites than the normal mucosa. In contrast, the signal intensity with Orc6-pT229 Ab showed enhanced expression at normal regions adjacent to the tumor (signal intensity of tumor to normal ~0.66-0.74), even though the number of positively stained cells was similar. These results support the model that phosphorylation of Orc6 functions like a "checkpoint-signal" during DNA damage to prevent cell cycle progression (Fig. 7C). The absence or reduction of Orc6 phosphorylation in tumor cells provides important insights into how Orc6 phosphorylation is vital for the maintenance of genome stability.

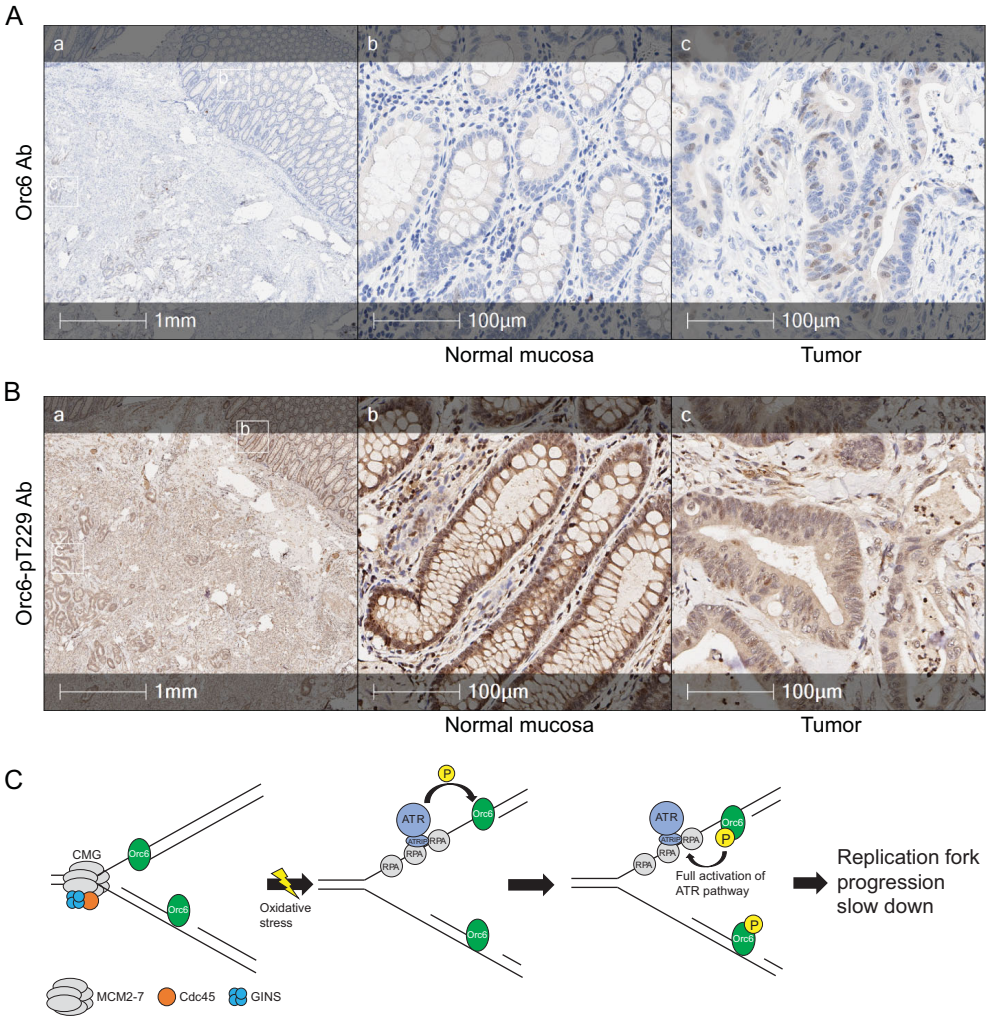

FIG 7 Localization of phosphorylated-Orc6 in cancer cells (A) Immunohistochemistry staining with Orc antibody. Tumor regions have more positively stained epithelial cells (a) slide with both tumor and normal mucosa (b) tumor region (c) normal mucosa). (B) Immunohistochemistry staining with Orc6-pT229 in colon carcinoma. Both tumor and normal regions have a similar number of positively stained cells, but cells in normal epithelium have more intense staining. (a) Low magnification view of tissue (b) high magnification view of normal mucosa (c) low magnification view of tissue (d) high magnification view of neoplastic glands in colon carcinoma. (C) Schematic model of the role of phospho-Orc6 at the fork during DNA damage.

DISCUSSION

It is known that yeast Orc6 not only functions in licensing but is also required after pre-RC formation, since depleting Orc6 after pre-RC formation destabilizes pre-RC and impairs origin firing.[33] We previously reported that human Orc6 functions after pre-RC formation, promotes S-phase progression and DNA damage response.[6] Further, Orc6 associates with the mismatch repair complex during the S-phase and modulates MMR complex assembly and activity. In this study, we report that in response to oxidative damage, Orc6 gets phosphorylated at T229 during S-phase and plays an important role in genome surveillance. Interestingly, overexpression of Orc6 and the phospho-dead mutant push cells towards the S-phase. Similarly, expression of the wild-type or phospho-dead Orc6 increases the ability of cancer cells to invade and migrate. However, the biochemical mechanism of Orc6 action remains to be determined.

The earliest steps of DNA replication, including pre-RC establishment, are coordinated with the DNA damage network that prevents genomic instability. ATR and Chk1 also restrain replication origin firing in normal cells and after DNA damage. Using stable isotope labeling by amino acids in cell culture (SILAC) quantitative proteomic approach, an earlier study identified over 700 ATM/ATR substrates upon IR-induced DNA damage, including hOrc6 at the Thr229 site.[18] Multiple pre-RC factors have also

been identified and studied. For example, Cdc6 physically interacts with ATR, which is thought to regulate the activation of the replication checkpoint.[34] Similarly, Mcm2 is an ATR substrate and associates with ATRIP. It is thought that the phosphorylation of MCM inhibits its DNA helicase activity or may contribute to maintaining MCM at the stalled fork to prevent fork collapse.[35] A potential mechanism to block re-replication after DNA damage could involve the phosphorylation of pre-RC components by one or several checkpoint kinases. We find that T229 of Orc6 is phosphorylated upon DNA damage, especially during oxidative stress, and is required for efficient ATR signaling activation. We propose that the phosphorylation of hOrc6 by ATM/ATR imposes a brake on DNA replication. In support of this, we find that cells expressing the phospho-mimetic mutant of Orc6 show reduced progression into S-phase (H_2O_2 treatment followed by release) and is unable to rescue the defect in replication progression (as measured by the DNA fiber assay). Migration assays showed that the phospho-mimetic mutant of Orc6 prevents tumor cell migration, supporting our argument that phosphorylation of Orc6 is a mechanism to prevent tumorigenesis. The phosphorylated hOrc6 either acts as a brake or as a sensor of oxidative DNA damage to prevent replication progression and tumorigenesis.

Metazoan Orc6 protein consists of N-terminal and middle domains with homology to the cyclin-box folds of the transcription factor (TFIIB).[8,36] The C-terminus of Orc6 that mediates its cytokinetic function was essential and sufficient for Orc6's interaction with Orc3 and for tethering Orc6 to the entire ORC.[3] Furthermore, a mutation within the C-terminus of Orc6 (hOrc6, tyrosine 232) is linked to Meier–Gorlin syndrome. Specific mutations within the hOrc6, as well as the corresponding mutations in *Drosophila* (Y225S or W228A/K229A; "YxxWK" motif) resulted in a loss of Orc6 binding to the ORC, decreased hexameric ORC formation, and MCM loading onto chromatin, and a consequent reduction in DNA synthesis.[3] Orc6 is phosphorylated in the budding yeast in a cell cycle-regulated manner to prevent re-replication. In human cells, the phosphorylation of Orc6 at Threonine 195 is implicated in its nuclear localization.[21,37] We found that upon H_2O_2-induced DNA damage, hOrc6 is phosphorylated at Thr229, which is adjacent to the 'YxxWK' conserved motif. Interestingly, the phospho-mimetic mutant of Orc6 displayed increased DNA binding activity, suggesting that hOrc6-pThr229 modification signals the cell to prevent fork progression until the damage is repaired. Earlier structural studies revealed that hOrc6's DNA binding ability lies within N-terminal TFIIB-like domain and not at the Thr229-containing C-terminal domain.[22,36] We predict that the difference in the DNA binding ability could be due to the conformational change and/or altered hOrc6 interactome of Orc6-pThr229. Future studies will identify the underlying mechanism responsible for pThr229-mediated differential binding of hOrc6 to DNA.

Together, our present study provides additional insights into the regulation of human Orc6 protein in cell cycle progression and DNA damage conditions, as well as its importance in cancer development and malignancy.

MATERIAL AND METHODS

Cell culture. All U2OS cell lines (U2OS WT, HA-Orc6-WT, HA-Orc6-T229A, HA-Orc6-T229E) are cultured in Dulbecco's modified Eagle's medium (DMEM) supplemented with high glucose and 5% fetal bovine serum (FBS). Constructed U2OS cell lines (HA-Orc6-WT, HA-Orc6-T229A, HA-Orc6-T229E) are selected by puromycin. M4 cell line (MCF10CA1a.cl1) is cultured in DMEM/F-12 medium supplemented with 5% horse serum (HS).[38] Plasmid DNAs were delivered by Lipofectamine/2000 or Lipofectamine 3000. siRNAs were delivered by Lipofectamine RNAimax. For cell synchronization, 50 ng/mL nocodazole treatment and release was used for M and G1 phase synchronization, while 2 mM thymidine block and release were used for G1/S, S and G2-phase synchronization.

Whole-cell lysis and immunoprecipitation. To prepare whole-cell lysate, cells were collected, washed with PBS and then lysed with lysis buffer (80 mM Tris pH6.9, 2% SDS, 15% glycerol, 0.1 M DTT) on ice for 15 min. Cell lysates were then mixed with loading dye and denatured at 95 °C for 5 min. Denatured protein samples were analyzed with western blot. Phos-tag analysis was done as mentioned in previous publication.[20]

For immunoprecipitation, cells were collected, washed with PBS and lysed in IP lysis buffer (50 mM Tris pH7.4, 150 mM NaCl, 1 mM $MgCl_2$, 10% glycerol, 0.2% NP-40) containing protease inhibitors. Lysates were then sonicated and treated with benzonase nuclease (Sigma) for 30 min at room temperature,

then EDTA was added to 2 mM. Centrifugation was done at 15,000 rpm for 10 min to remove insoluble debris. Next, lysates were pre-cleared with Gammabind G sepharose (GE healthcare Life Science) for 30 min at 4 °C. Antibodies were then added into lysates and incubated at 4 °C overnight. Proteins bound by antibodies were pulled down by Gammabind G Sepharose for 3h at 4 °C. After incubation, beads were washed in lysis buffer and captured proteins were eluted and analyzed with western blot.

The list of antibodies and reagents used in this study are included as Supplementary Table 1.

***In Situ* protein interactions at replication forks (SIRF).** For SIRF experiments,[39] cells were first pulsed with 125 μM EdU for 10 min. For thymidine chases, cells were washed with PBS then 100 μM of thymidine was added for 4 h. Cells were then fixed in 2% paraformaldehyde (PFA) for 15 min at room temperature and permeabilized on ice with PBS containing 0.5% Triton X-100. After washing with PBS, click reaction was performed with biotin-azide for 1 h at room temperature. To select cells with EdU incorporation, the biotin-azide was supplemented with Alexa Flour-488-azide at a proportion of 1:9. The coverslips were then blocked with blocking solution and preceded to standard PLA procedure using antibiotin and antibodies indicated in the figures. PLA was performed using Sigma Duolink PLA as per the manufacturer's protocol.

Single molecule pull down (SiMPull). For replication fork-like DNA substrate preparation, partial duplexes of T1/P1 and T2/P2 were generated by annealing equimolar concentrations of the oligonucleotides in a buffer containing 10 mM Tris, pH 8.0 and 50 mM NaCl at 95 °C for 3 min, followed by slow cooling to room temperature. The two duplexes were then combined together and incubated overnight at room temperature to generate the replication fork probe. The reaction mixture was subjected to PAGE purification prior to use.

For double-strand DNA substrate, a T1-int/T2 duplex was generated similarly by annealing T1-int and T2 at 95 °C for 3 min, slow cooling to ambient temperature, followed by PAGE purification. The purified constructs were stored in buffer containing 10 mM Tris, pH 8.0 and 25 mM NaCl.

Single-molecule experiments were performed on a prism-type TIRF microscope equipped with an electron-multiplying CCD camera (EM-CCD).[40] For single-molecule pull-down experiments quartz slides and glass cover slips were passivated with 5000 MW methoxy poly-(ethylene glycol) (mPEG, Laysan Bio) doped with 2–5% 5000 MW biotinylated PEG (Laysan Bio). Each passivated slide and cover slip was assembled into flow chambers. GST-Flag-Orc6 wild-type and its variants (T229A and T229E) were diluted to 1 nM and pulled down with biotinylated antibodies against GST (Abcam, ab87834), already immobilized on the surface via neutravidin-biotin linkage. Any unbound protein was washed off after 10 min incubation and a predefined concentration of DNA substrate (replication fork-DNA, dsDNA, i.e. T1-int/T2 or ssDNA, i.e. T1-int) was introduced in the imaging chamber. The protein-DNA complexes were imaged post 15 min incubation with the DNA substrate, in a buffer containing 20 mM HEPES (pH 8), 60 mM KCl, 5 mM MgCl2, 0.5 mM EDTA and 8% glycerol. Cy3- and Cy5- tagged DNA were excited at 532 nm and 640 nm respectively and the emitted fluorescence signal was collected via band pass filters (HQ 570/40, Semrock for Cy3 and 665LP, Semrock for Cy5). Fifteen frames were recorded from each of 20 different imaging areas (5,000 μm^2) and isolated single-molecule peaks were identified by fitting a Gaussian profile to the average intensity from the first 10 frames. Mean spot-count per image for Cy3 and Cy5 was obtained by averaging 20 imaging areas using MATLAB scripts. All experiments were carried out at room temperature.

Flow cytometry. For PI cell cycle profile, cells were collected and washed once in ice cold PBS, resuspended in PBS + 1% NGS, and fixed in 90% chilled ethanol at 4 °C overnight. Cells were then washed and resuspended in PBS + 1% NGS with 120 μg/mL propidium iodide (PI) and 10 μg/mL RNase A for 45 min at 37 °C. DNA content was measured by flow cytometry. Data were processed in FCS Express 5.

DNA fiber assay. U2OS cells were labeled with 50 μm CldU and 200 μm IdU according to the scheme in Fig. 3C prior to collection. DNA fibers were prepared on vinyl-silane coated coverslips using the FiberComb molecular combing system (Genomic Vision) as per the manufacturer's protocol. The visualization procedures of CldU and IdU tracks were based on previous work in Jensen Lab.[41] DNA fibers were denatured in denature solution (0.5 M NaOH, 1 M NaCl) for 8 min at room temperature, washed three times in PBS, then dehydrated in 70% and 100% ethanol for 5 min each. Dried coverslips were blocked in 5% BSA/PBS at 37 °C for 30 min, then incubated with mouse anti-BrdU (BD Biosciences, 1:10) and rat anti-BrdU (Bio-Rad, 1:40) at 37 °C for 1 h. After washing in PBS, coverslips were incubated in FITC-conjugated goat anti-rat IgG and Texas Red-conjugated goat anti-mouse IgG at 37 °C for 30–60 min. After final washes in PBS, the coverslips were mounted with Ibidi Mounting medium (Ibidi, #50001). The images were captured using Zeiss Axiovision system, and length of IdU tracks were quantified using ImageJ software.

Transwell migration and invasion assays. For migration assay, Orc6-depleted U2OS or M4 cells were pre-starved with serum-free culture medium for 5 h (see "Cell culture" section). Cells were then seeded onto the top of 8.0 μm migration chamber (Corning), with complete medium on the other side of chamber. Cells were allowed to migrate for 24 h at 37 °C. Following that, the unmigrated cells were scrubbed. The migrated cells were fixed with prechilled absolute methanol for 5 min, stained with 0.05% crystal violet in 10% methanol for 30 min, washed with water and left dry before imaging. Same procedures above were done for invasion assay. Instead of the migration chamber, Matrigel-coated invasion chamber (Corning) was used. Quantifications of cell images were processed in ImageJ.

Immunohistochemistry. Tissue received from the UI Biorepository was sectioned at 5 μm, baked, deparaffinized and stained on BOND RX automated stainer (Leica Biosystems) using BOND Polymer Refine Detection (Leica, #DS9800) and BOND Research Detection (DS#9455) kits. Sections were subjected to antigen retrieval for 40 min at 100 °C with citric acid-based (BOND ER1 solution, pH6, #AR9961) for

pOrc6 staining or for 90 min at 100 °C with EDTA-based (BOND ER2 solution, pH9, #AR9640) for Orc6 staining. Endogenous peroxidase activity and nonspecific binding was blocked by treating samples with peroxidase block (3% H_2O_2 in methanol) and protein block (Background Sniper, Biocare Medical, #BS966) for 30 min at room temperature (RT) respectively. Sections were then incubated with 1:8000 pORC6 antibody or with 1:25 Orc6 antibody (Santa Cruz Biotechnology, #sc-32735). After several washes, the signal detection was performed with the reagents from the Polymer Refine kit mentioned above for pOcr6 antibody or with anti-rat HRP polymer (cell Idx, #2AH-015) combined with Betazoid DAB Chromogen Kit (Biocare Medical,# BDB2004) for Orc6 antibody. All sections were then counterstained with hematoxylin for 10 min and mounted with Micromount media (Leica Microsystems, #3801730).

Slides were scanned at 20× on an Aperio AT2 scanner (Leica Biosystems, Deer Park, IL). The resulting images were analyzed using HALO AI analysis software (Indica Labs, Albuquerque, NM). Tumor and normal mucosa regions were annotated by a pathologist. Then, epithelial tissue was identified using a custom-trained HALO AI MiniNet tissue classifier. Signal intensity was determined using the Halo Multiplex IHC module. An artificial-intelligence algorithm was used to segment individual cells within the epithelial tissue. Color deconvolution was used to separate DAB and hematoxylin and generate an optical density for each stain in each cell.

SUPPLEMENTAL MATERIAL

Supplemental data for this article can be accessed online at https://doi.org/10.1080/10985549.2023.2196204.

ACKNOWLEDGEMENTS

We thank members of the Prasanth laboratory for discussions and suggestions. We thank Drs M. Aladjem, R. Bhargava, J. Cook, A. Dutta, H. Ducoff (posthumous), R. Hsu, M. Mechali, B. Moriarity, S. Nair, B. Stillman, M. Sverdlov, Y. Wang, M. Wold, L. Zou for providing reagents and insightful suggestions. This work was supported by NIH [R35 GM 122569] and NSF [PHY 1430124] awards to TH; NIH [R21AG065748; R01GM132458], Cancer center at Illinois seed grant and Prairie Dragon Paddlers awards [MCB1723008] to KVP; and NSF [1243372, 1818286, 2225264], NIH [GM125196] and CCIL awards to SGP. TH is an investigator with Howard Hughes Medical Institute.

AUTHOR CONTRIBUTIONS

Y-C.L., D.L. and A.C. designed, performed, and analyzed most experiments. J.S. helped with IP experiments; J.M. did SiMPull experiments; V.M, E.B, and A.K-B. did the IHC staining and analyses; L.S. did the invasion and migration experiment in M4 cells; T.H. provided technical support and conceptual advice toward SiMPull experiments. S.G.P. and K.V.P. supervised the project. Y-C.L., D.L., and S.G.P. wrote the manuscript.

ORCID

Supriya G. Prasanth http://orcid.org/0000-0002-3735-7498

DATA AVAILABILITY STATEMENT

The data supporting the findings of this study are available within the article and in the supplementary material. No new datasets were generated in this study.

REFERENCES

1. Bell SP, Dutta A. DNA replication in eukaryotic cells. Annu Rev Biochem. 2002;71:333–374.
2. Bell SP, Stillman B. ATP-dependent recognition of eukaryotic origins of DNA replication by a multiprotein complex. Nature. 1992;357:128–134.
3. Bleichert F, Balasov M, Chesnokov I, Nogales E, Botchan MR, Berger JM. A Meier-Gorlin syndrome mutation in a conserved C-terminal helix of Orc6 impedes origin recognition complex formation. Elife. 2013;2:e00882.
4. Li N, Lam WH, Zhai Y, Cheng J, Cheng E, Zhao Y, Gao N, Tye BK. Structure of the origin recognition complex bound to DNA replication origin. Nature. 2018;559:217–222. doi:10.1038/s41586-018-0293-x.
5. Miller TCR, Locke J, Greiwe JF, Diffley JFX, Costa A. Mechanism of head-to-head MCM double-hexamer formation revealed by cryo-EM. Nature. 2019;575:704–710. doi:10.1038/s41586-019-1768-0.
6. Lin YC, Liu D, Chakraborty A, Kadyrova LY, Song YJ, Hao Q, Mitra J, Hsu RYC, Arif MK, Adusumilli S, et al. Orc6 is a component of the replication fork and enables efficient mismatch repair. Proc Natl Acad Sci U S A. 2022;119:e2121406119.
7. Bernal JA, Venkitaraman AR. A vertebrate N-end rule degron reveals that Orc6 is required in mitosis for daughter cell abscission. J Cell Biol. 2011;192:969–978.
8. Chesnokov IN, Chesnokova ON, Botchan M. A cytokinetic function of Drosophila ORC6 protein resides in a domain distinct from its replication activity. Proc Natl Acad Sci U S A. 2003;100:9150–9155.
9. Prasanth SG, Prasanth KV, Stillman B. Orc6 involved in DNA replication, chromosome segregation, and cytokinesis. Science. 2002;297:1026–1031.
10. Cook JG. Replication licensing and the DNA damage checkpoint. Front Biosci (Landmark Ed). 2009;14:5013–5030.
11. Marechal A, Zou L. DNA damage sensing by the ATM and ATR kinases. Cold Spring Harb Perspect Biol. 2013;5:a012716.
12. Lee JH, Paull TT. ATM activation by DNA double-strand breaks through the Mre11-Rad50-Nbs1 complex. Science. 2005;308:551–554. doi:10.1126/science.1108297.
13. Shiotani B, Zou L. Single-stranded DNA orchestrates an ATM-to-ATR switch at DNA breaks. Mol Cell. 2009;33:547–558.

14. Cook JG. Eplication licensing and the DNA damage checkpoint. Front Biosci. 2009;14:5013–5030.
15. Hurley PJ, Bunz F. ATM and ATR - components of an integrated circuit. Cell Cycle. 2007;6:414–417.
16. Ge XQ, Jackson DA, Blow JJ. Dormant origins licensed by excess Mcm2-7 are required for human cells to survive replicative stress. Genes Dev. 2007;21:3331–3341. English.
17. Woodward AM, Gohler T, Luciani MG, Oehlmann M, Ge XQ, Gartner A, Jackson DA, Blow JJ. Excess Mcm2-7 license dormant origins of replication that can be used under conditions of replicative stress. J Cell Biol. 2006;173:673–683. doi:10.1083/jcb.200602108.
18. Matsuoka S, Ballif BA, Smogorzewska A, McDonald ER 3rd, Hurov KE, Luo J, Bakalarski CE, Zhao Z, Solimini N, Lerenthal Y, et al. ATM and ATR substrate analysis reveals extensive protein networks responsive to DNA damage. Science. 2007;316:1160–1166.
19. Nguyen VQ, Co C, Li JJ. Cyclin-dependent kinases prevent DNA re-replication through multiple mechanisms. Nature. 2001;411:1068–1073. doi:10.1038/35082600.
20. Chakraborty A, Prasanth KV, Prasanth SG. Dynamic phosphorylation of HP1alpha regulates mitotic progression in human cells. Nat Commun. 2014;5:3445.
21. Ghosh S, Vassilev AP, Zhang J, Zhao Y, DePamphilis ML. Assembly of the human origin recognition complex occurs through independent nuclear localization of its components. J Biol Chem. 2011;286:23831–23841. doi:10.1074/jbc.M110.215988.
22. Balasov M, Huijbregts RP, Chesnokov I. Role of the Orc6 protein in origin recognition complex-dependent DNA binding and replication in *Drosophila melanogaster*. Mol Cell Biol. 2007;27:3143–3153.
23. Xu N, You Y, Liu C, Balasov M, Lun LT, Geng Y, Fung CP, Miao H, Tian H, Choy TT, et al. Structural basis of DNA replication origin recognition by human Orc6 protein binding with DNA. Nucleic Acids Res. 2020;48:11146–11161.
24. Jain A, Liu R, Ramani B, Arauz E, Ishitsuka Y, Ragunathan K, Park J, Chen J, Xiang YK, Ha T. Probing cellular protein complexes using single-molecule pull-down. Nature. 2011;473:484–488.
25. Techer H, Koundrioukoff S, Azar D, Wilhelm T, Carignon S, Brison O, Debatisse ML, Tallec B. Replication dynamics: biases and robustness of DNA fiber analysis. J Mol Biol. 2013;425:4845–4855.
26. Chen H, Bao L, Hu J, Wu D, Tong X. ORC6, negatively regulated by miR-1-3p, promotes proliferation, migration, and invasion of hepatocellular carcinoma cells. Front Cell Dev Biol. 2021;9:652292.
27. Hu Y, Wang L, Li Z, Wan Z, Shao M, Wu S, Wang G. Potential prognostic and diagnostic values of CDC6, CDC45, ORC6 and SNHG7 in colorectal cancer. Onco Targets Ther. 2019;12:11609–11621.
28. Idilli AI, Pagani F, Kerschbamer E, Berardinelli F, Bernabé M, Cayuela ML, Piazza S, Poliani PL, Cusanelli E, Mione MC. Changes in the expression of pre-replicative complex genes in hTERT and ALT pediatric brain tumors. Cancers (Basel). 2020;12:1028.
29. Pan Q, Li F, Ding Y, Huang H, Guo J. ORC6 acts as a biomarker and reflects poor outcome in clear cell renal cell carcinoma. J Cancer. 2022;13:2504–2514.
30. Koleck TA, Conley YP. Identification and prioritization of candidate genes for symptom variability in breast cancer survivors based on disease characteristics at the cellular level. Breast Cancer. 2016;8:29–37.
31. Xi Y, Formentini A, Nakajima G, Kornmann M, Ju J. Validation of biomarkers associated with 5-fluorouracil and thymidylate synthase in colorectal cancer. Oncol Rep. 2008;19:257–262.
32. Gavin EJ, Song B, Wang Y, Xi Y, Ju J. Reduction of Orc6 expression sensitizes human colon cancer cells to 5-fluorouracil and cisplatin. pLoS One. 2008;3:e4054.
33. Semple JW, Da-Silva LF, Jervis EJ, Ah-Kee J, Al-Attar H, Kummer L, Heikkila JJ, Pasero P, Duncker BP. An essential role for Orc6 in DNA replication through maintenance of pre-replicative complexes. Embo J. 2006;25:5150–5158.
34. Yoshida K, Sugimoto N, Iwahori S, Yugawa T, Narisawa-Saito M, Kiyono T, Fujita M. CDC6 interaction with ATR regulates activation of a replication checkpoint in higher eukaryotic cells. J Cell Sci. 2010;123:225–235. English. doi:10.1242/jcs.058693.
35. Cortez D, Glick G, Elledge SJ. Minichromosome maintenance proteins are direct targets of the ATM and ATR checkpoint kinases. Proc Natl Acad Sci U S A. 2004;101:10078–10083.
36. Liu S, Balasov M, Wang H, Wu L, Chesnokov IN, Liu Y. Structural analysis of human Orc6 protein reveals a homology with transcription factor TFIIB [Comparative Study Research Support, N.I.H., Extramural Research Support, Non-U.S. Gov't]. Proc Natl Acad Sci USA. 2011;108(18):7373–7378.
37. Honey S, Futcher B. Roles of the CDK phosphorylation sites of yeast Cdc6 in chromatin binding and rereplication. Mol Biol Cell. 2007;18:1324–1336.
38. Jadaliha M, Gholamalamdari O, Tang W, Zhang Y, Petracovici A, Hao Q, Tariq A, Kim TG, Holton SE, Singh DK, et al. A natural antisense lncRNA controls breast cancer progression by promoting tumor suppressor gene mRNA stability. pLoS Genet. 2018;14:e1007802.
39. Roy S, Luzwick JW, Schlacher K. SIRF: Quantitative in situ analysis of protein interactions at DNA replication forks. J Cell Biol. 2018;217:1521–1536.
40. Roy R, Hohng S, Ha T. A practical guide to single-molecule FRET. Nat Methods. 2008;5:507–516.
41. Moore GJ, Sainz J, Jensen RB. DNA fiber combing protocol using in-house reagents and coverslips to analyze replication fork dynamics in mammalian cells. STAR Protoc. 2022;3:101371.